HHS Public Access

Author manuscript

Neurobiol Dis. Author manuscript; available in PMC 2021 April 23.

Published in final edited form as:

Neurobiol Dis. 2020 December ; 146: 105085. doi:10.1016/j.nbd.2020.105085.

Divergent FUS phosphorylation in primate and mouse cells following double-strand DNA damage

Michelle A. Johnson[a,b], **Qiudong Deng**[a,b], **Georgia Taylor**[a,b], **Zachary T. McEachin**[b,d,e], **Anthony W.S. Chan**[b,f,g], **Jessica Root**[a,b], **Gary J. Bassell**[b,d,e], **Thomas Kukar**[a,b,c,*]

[a]Department of Pharmacology and Chemical Biology, Emory University, School of Medicine, Atlanta, GA, United States of America

[b]Center for Neurodegenerative Disease, Emory University, School of Medicine, Atlanta, GA, United States of America

[c]Department of Neurology, Emory University, School of Medicine, Atlanta, GA, United States of America

[d]Department of Cell Biology, Emory University, School of Medicine, Atlanta, GA, United States of America

[e]Laboratory of Translational Cell Biology, Emory University, School of Medicine, Adanta, GA, United States of America

[f]Department of Human Genetics, Emory University, School of Medicine, Atlanta, GA, United States of America

[g]Division of Neuropharmacology and Neurologic Diseases, Yerkes National Primate Research Center, 954 Gatewood Rd, NE, Atlanta, GA, United States of America

Abstract

Fused in sarcoma (FUS) is a RNA/DNA protein involved in multiple nuclear and cytoplasmic functions including transcription, splicing, mRNA trafficking, and stress granule formation. To accomplish these many functions, FUS must shuttle between cellular compartments in a highly regulated manner. When shuttling is disrupted, FUS abnormally accumulates into cytoplasmic inclusions that can be toxic. Disrupted shuttling of FUS into the nucleus is a hallmark of ~10% of frontotemporal lobar degeneration (FTLD) cases, the neuropathology that underlies frontotemporal dementia (FTD). Multiple pathways are known to disrupt nuclear/cytoplasmic shuttling of FUS. In earlier work, we discovered that double-strand DNA breaks (DSBs) trigger DNA-dependent protein kinase (DNA-PK) to phosphorylate FUS (p-FUS) at N-terminal residues leading to the cytoplasmic accumulation of FUS. Therefore, DNA damage may contribute to the

*Corresponding author at: Department of Pharmacology and Chemical Biology, Emory University, 1510 Clifton Rd, Suite 5123, Atlanta, GA 30322, United States of America. Thomas.Kukar@emory.edu (T. Kukar).

Declaration of Competing Interest

The authors declare that they have no known competing financial interests or personal relationships that could have appeared to influence the work reported in this paper.

Appendix A. Supplementary data

Supplementary data to this article can be found online at https://doi.org/10.1016/j.nbd.2020.105085.

development of FTLD pathology with FUS inclusions. In the present study, we examined how DSBs effect FUS phosphorylation in various primate and mouse cellular models. All cell lines derived from human and non-human primates exhibit N-terminal FUS phosphorylation following calicheamicin γ1 (CLM) induced DSBs. In contrast, we were unable to detect FUS phosphorylation in mouse-derived primary neurons or immortalized cell lines regardless of CLM treatment, duration, or concentration. Despite DNA damage induced by CLM treatment, we find that mouse cells do not phosphorylate FUS, likely due to reduced levels and activity of DNA-PK compared to human cells. Taken together, our work reveals that mouse-derived cellular models regulate FUS in an anomalous manner compared to primate cells. This raises the possibility that mouse models may not fully recapitulate the pathogenic cascades that lead to FTLD with FUS pathology.

Keywords

Frontotemporal dementia (FTD); Amyotrophic lateral sclerosis (ALS); Fused in sarcoma (FUS); DNA-dependent protein kinase (DNA-PK); DNA damage; Phosphorylation; Calicheamicin γ1 (CLM); Species specific response

1. Introduction

Frontotemporal dementia (FTD) is the most common form of dementia in people under the age of 60 and the third most common form of dementia in the United States overall (Boxer et al., 2020; Hodges et al., 2003; Knopman and Roberts, 2011; Vieira et al., 2013). Although a heterogeneous disorder, FTD symptoms typically include progressive deficits in behavior, executive function, and/or language (Bang et al., 2015). The neuropathology underlying FTD is called frontotemporal lobar degeneration (FTLD). FTLD is defined by neurodegeneration, gliosis and microvascular changes within the frontal and/or anterior temporal brain cortices (Bahia et al., 2013; Mackenzie et al., 2009; Mackenzie et al., 2010). FTLD is further subdivided into groups based on the major protein found in neuronal and glial inclusions. The four subgroups of FTLD are defined by the abnormal accumulation of the following proteins: 1) tau, 2) TAR DNA-binding protein 43 (TDP-43), 3) the FET (FUS, EWS, TAF-15) proteins, or 4) ubiquitin/proteasome system proteins (FTLD-tau, FTLD-TDP, FTLD-FET, and FTLD-UPS, respectively) (Neumann and Mackenzie, 2019). While the majority of FTLD cases have tau or TDP-43 pathology (36–50% and ~50%, respectively), a significant proportion of FTLD cases have inclusions containing the FET proteins (~10%) (Neumann et al., 2009).

The FET family of proteins includes fused in sarcoma (FUS), Ewing's sarcoma (EWS), and TATA binding protein-associated factor 15 (TAF-15) (Andersson et al., 2008). FUS, EWS, and TAF-15 are ubiquitously expressed, multi-functional RNA/DNA binding proteins (Deng et al., 2014a). FUS was the first FET protein linked to FTD (Kwiatkowski et al., 2009; Neumann et al., 2009; Vance et al., 2009). Like the other FET proteins, FUS contains three characteristic domains: a low complexity SYGQ domain, a 3-glycine/arginine rich RGG domains, and a zinc finger domain (Andersson et al., 2008; Svetoni et al., 2016). FUS utilizes these domains to facilitate multiple cellular functions in both the cytoplasm and

nucleus including DNA transcription, RNA translation, mRNA splicing, stress granule formation, and DNA repair (De Santis et al., 2017; Fujii et al., 2005; Kamelgarn et al., 2016; Sama et al., 2014; Schwartz et al., 2012; Shelkovnikova et al., 2013; Tan et al., 2012; Yang et al., 2014; Zinszner et al., 1997). Given this diverse set of functions, FUS must shuttle rapidly between the nucleus and cytoplasm of the cell. However, in FTLD-FET, disrupted nuclear/cytoplasmic shuttling causes FUS to accumulate into insoluble cytoplasmic inclusions. Multiple studies have shown that FUS-positive cytoplasmic inclusions can trigger a toxic gain-of-function that leads to cell death in a concentration dependent manner (Deng et al., 2014a; Mitchell et al., 2012; Scekic-Zahirovic et al., 2016). In other words, the more FUS that accumulates in the cytoplasm, the greater the toxicity.

Pathogenic *FUS* mutations almost invariably cause ALS (Renton et al., 2014). FTD caused by a *FUS* mutation is extremely rare or leads to a combined FTD-ALS presentation (Broustal et al., 2010; Rohrer et al., 2009; Snowden et al., 2011). For that reason, FTLD-FET pathogenesis is thought to primarily occur independent of genetic factors, and may instead be the result of broader impairments in the transport or function of these RNA-binding proteins (Darovic et al., 2015; Deng et al., 2014a; Dormann et al., 2012; Gami-Patel et al., 2016; Niu et al., 2012; Ravenscroft et al., 2013). In line with this idea, various non-genetic models of FUS transport deficits have been described including changes in methylation status, loss of transportin-1/FUS interaction, cellular stress events, and phosphorylation (Bowden and Dormann, 2016; Darovic et al., 2015; Dormann et al., 2012; Higelin et al., 2016; Sama et al., 2013; Scaramuzzino et al., 2013; Singatulina et al., 2019; Verbeeck et al., 2012). Previous studies from our lab and others have shown that double-stranded DNA damage induces phosphorylation of N-terminal residues in FUS (Deng et al., 2014b; Monahan et al., 2017; Rhoads et al., 2018a). Following this event, we have shown that p-FUS begins to accumulate in the cytoplasm of the cell (Deng et al., 2014b). Evidence suggests that DNA damage is a common hallmark of FUS protein pathology (Deng et al., 2014b; Higelin et al., 2016; Naumann et al., 2018). Therefore, DNA damage induced N-terminal phosphorylation may be a critical pathological event leading to FUS cytoplasmic accumulation and toxicity.

Here, we aimed to study FUS phosphorylation in mouse primary cellular models because they are a tractable and scalable model that have been used to study neurodegeneration in other contexts. Surprisingly, we were unable to detect FUS phosphorylation following calicheamicin-γ1 (CLM) induced double-strand DNA damage in primary mouse neurons. Further, we found that mouse-derived immortalized cell lines show no detectable phosphorylation of FUS or cytoplasmic accumulation in response to CLM treatment. Our data suggests that decreased expression and activity of the DNA-dependent protein kinase (DNA-PK) in mouse cells compared to human cells may underlie the species-specific difference we observed. These data indicate that there are fundamental differences in DNA damage and repair pathways between rodents and primates.

2. Materials and methods

2.1. Cell culture

2.1.1. Primary mouse neurons—All animal experiments were reviewed and approved by the Institutional Animal Care and Use Committees at Emory in accordance with the National Institutes of Health Guide for the Care and Use of Laboratory Animals. Mouse primary cortical neurons were isolated and cultured according to a previously described procedure (Sala et al., 2000). In brief, mouse primary cortical neurons were isolated from E18 C57BL/6 mouse brain cortices, plated on 12-well plates and cultured in neurobasal medium (Giboco) containing 2% B27 (GIBCO). Neurons were used 7–14 days after plating. The cultures were maintained at 37 °C in a 5% CO_2 incubator. The culture medium was changed with the same solution 24 h after plating and then half-changed once every week.

2.1.2. Nonhuman primate induced pluripotent stem cells (iPSCs), neural progenitor cells, and differentiated cells—Wild type non-human primate induced pluripotent stem cells (iPSCs), neural progenitor cells (NPC), differentiated neurons were generated and cultured as published (Carter et al., 2014; Cho et al., 2019a; Cho et al., 2019b). In brief, iPSCs were dissociated from MEF feeder layers and were cultured in MEF-conditioned ES cell medium without bFGF (R&D). After 7 days, ES cell medium was replaced with derivation medium. After another 7 days, neurospheres were plated on P/L-coated cell culture dishes and expanded in neural proliferation medium. After 7–10 days, neural rosettes were manually picked and seeded onto fresh cell culture dishes in differentiation medium. Cells were finally differentiated with the supplement of SHH and FGF and ascorbic acid.

2.1.3. Human-derived iPSC maintenance and motor neuron differentiation—A control iPS cell line was maintained on Matrigel coated dishes and fed every day with mTesRl medium (Stem Cell Technologies). Cells were passaged every 5–7 days using ReLesR passaging reagent. For differentiation to motor neurons, iPSC colonies were treated with 10 μM ROCK inhibitor, Y-27632 (Stem Cell Technologies), for ~1 h before being dissociated to single cells using Accutase (Stem Cell Technologies) for ~8 min. Cells were resuspended in motor neuron differentiation medium (1:1 Advanced DMEM-F12/ Neurobasal, IX N2, IX B27, 0.2% penicillin/streptomycin (Pen/Strep), IX Glutamax, 110 μM β-mercaptoethanol) and seeded in 10 cm Ultra-Low Attachment dishes (Corning) in order to form embryoid bodies. Cells were maintained as embryoid bodies throughout the differentiation procedure and were fed every 2 days. The differentiation medium contained 3 μM CHIR99021 (Stem Cell Technologies), 10 μM SB431542 (Stem Cell Technologies), 10 μM DMH1, and 10 μM Y-27632. On Day 2, 1 μM Retinoic Acid (Sigma) and 500 nM Smoothened Agonist (Millipore) were added to the differentiation medium. CHIR99021 was removed from the medium on Day 6 and SB and DMH1 were removed from the medium on Day 10. Subsequently, on Day 14, 10 ng/mL BDNF (Peprotech), 10 ng/mL GDNF (Peprotech), and 10 μM DAPT (Tocris) were added. On day 20, embryoid bodies were disassociated to single cells using papain/DNase (Worthington Bio) and plated on polyornithine/laminin coated cell culture plates.

2.1.4. Human neurons—Human neurons were purchased from ScienCell and cultured according to manufacturer recommendations (ScienCell, #1520).

2.1.5. Immortalized cell lines—Human neuroglioma cells (H4; ATCC) were cultured in Opti-MEM medium plus 5% fetal bovine serum (FBS) and 1% Pen/Strep. Human embryonic kidney cells (HEK293T; ATCC) and mouse embryonic fibroblasts (MEF; kindly provided by Dr. Bob Farese) were cultured in DMEM medium plus 10% FBS and 1% Pen/Strep (Gibco). Human SH-SY5Y cells (SH-SY5Y; ATCC) and mouse Neuro2A (N2A; ATCC) cells were cultured in MEM medium plus 1% Pen/Strep and either 15% FBS and 10% FBS, respectively. All cultures were maintained at 37 °C with 5% CO_2.

2.2. Drug treatments

Calicheamicin γ1 (CLM) was obtained from Pfizer. Staurosporine was purchased from Cell Signaling Technologies (CST; #9953). Calyculin A (Cal A) was purchased from Cell Signaling Technology (CST; #9902). All drugs were resuspended in DMSO and aliquoted and stored at either −20 °C or −80 °C until use. Cells were plated into 60 mm dishes and dosed 72 h later at between 70 and 85% confluency.

2.3. Cell transfection

Mouse and human GFP-FUS plasmids were obtained from Dr. Keith W. Caldecott. HEK293T and N2A cells were plated into 6-well plate and allowed to grow overnight. The next day, cells were transfected with 2.5 μg of mouse GFP-FUS or human GFP-FUS DNA using the TransIT®-LT1 Transfection Reagent (Mirus; MIR2300). Cells were allowed to express plasmids for 24 h before treatment.

2.4. Western blotting

Cell lysis and western blotting was performed as previously described with minor modifications (Holler et al., 2017). In brief, cells were lysed on ice in either RIPA Buffer (50 mM tris pH = 8.0, 150 mM NaCl, 0.1% SDS, 1% trition-x-100, 0.5% sodium deoxycholate) or cytoplasmic lysis buffer (50 mM tris pH = 8.0, 150 mM NaCl, 0.5% trition-x-100) with 1% protein/phosphatase inhibitor (ThermoFisher; 78,442). The RIPA lysate was sonicated and centrifuged for 15 min at 14,000 rpm at 4 °C. The cytoplasmic lysate was vortexed and centrifuged for 15 min at 14,000 rpm at 4 °C. The supernatant was saved as the detergent soluble protein fraction. Protein concentration were measured in the detergent soluble protein fraction by BCA assay (Pierce). Next, cell lysates were analyzed for relative protein expression using SDS/PAGE followed by two-channel infrared quantitative western blots as described previously (Deng et al., 2014b). The samples were denatured in 1X Laemmli loading buffer with 5% tris(2-carboxyethyl) phosphine (TCEP) at 70 °C for 15 min. Equal amounts of protein were loaded into either a 4–20% or 12% PROTEAN TGX Precast Gels (Bio-Rad) or a 8% SurePAGE Bis-Tris precast gel (GenScript). After transferring to 0.2 μm nitrocellulose membranes, blots were stained with Revert 700 (LI-COR; 926–11,010) to measure total protein for normalization, captured at 700 nm on an Odyssey Fc Imaging System (LI-COR), then destained following the manufacture's protocol. Protein blots were then blocked in Odyssey or Intercept blocking buffer in TBS (LI-COR; 927–500,000 or 927–60,001, respectively) for 1 h at room temperature and incubated with primary

antibodies (diluted in 1:1 blocking buffer and TBS plus 0.2% Tween 20) overnight at 4 °C. Membranes were washed three times for five minutes in TBST and then incubated with the appropriate secondary antibody diluted in 10% blocking buffer diluted in TBS plus 0.1% Tween 20 (TBST) for 60 min at room temperature. Membranes were then washed three times with TBST for five minutes and visualized using the Odyssey Fc Imaging System (LI-COR). The following primary antibodies were used: FUS (1:1000; Santa Cruz; sc47711), FUS (1:2000; Bethyl Laboratories; A300-302A), phospho-ATR/ATM Substrate Motif [(pS/pT) QG] (1:1000; Cell Signaling Technologies; 6966), H2AX (1:1000; Millipore; AB10022), P-H2AX (1:1000; Millipore; 05–636), GAPDH (1:10,000; Cell Signaling Technologies; 2118), Mouse Specific cleaved PARP (1:1000; Cell Signaling Technologies; 9544), tubulin (1:20,000; Epitomics), total DNA-PK (1:500; ThermoFisher; PA5-86134), and p-DNA-PK (S2056) (1:1000; Abcam; ab18192). p-FUS (Ser30) antibody was kindly provided by Dr. Frank Shewmaker (Rhoads et al., 2018a). The following secondary antibodies were used: Donkey anti-mouse IgG Alexa Fluor Plus 680 (1:10,000; ThermoFisher; A32788) and Donkey anti-rabbit IgG Alexa Fluor Plus 800 (1:10,000; ThermoFisher; A32808).

2.5. Immunofluorescence

Following CLM treatment, cells were washed three times at room temperature with DPBS and fixed in 4% paraformaldehyde for 15 min. After washing, cells were permeabilized in −20 °C 100% methanol for 5 min. Cells were then washed three times in DPBS and blocked in 3% BSA for 1 h at room temperature. After blocking, cells were incubated overnight at 4 °C in primary antibody diluted in blocking buffer. The next day cells were washed three times with DPBS and incubated in Goat anti-rabbit 488 secondary antibody diluted in blocking buffer (1:400; ThermoFisher; A-21206). Following incubation, cells were washed three times in DPBS and mounted onto glass slides using Prolong Gold with DAPI (ThermoFisher; P36935). The following primary antibodies were used: total DNA-PK (1:200; ThermoFisher; PAS-86134), and p-DNA-PK (S2056) (1:200; Abcam; ab18192).

2.6. Image analysis

Following the above staining protocol, images were collected on a Leica DMi8 THUNDER Inverted Fluorescence Microscope with a DFC7000 T camera (Leica). Quantified images were collected at 20X (HC PL FLUOTAR L 20X/0.4 Dry); representative images were collected at 63X (HC PL APO 63X/1.400.60 Oil). For quantified images, images were collected at four randomized points/condition for all three replicates. Microscope settings including gain, exposure time, and LED intensity were identical between cell lines. All images for both cell lines were collected during the same day. Images were processed in the open source software, Fiji (Schindelin et al., 2012; Schneider et al., 2012). In brief, all images were background subtracted using the rolling ball macro, followed by application of a gaussian blur of 2 sigma, and automatic thresholding using the Otsu dark method. Average signal intensity of goat anti-rabbit 488 secondary antibody (termed “Total DNA-PK”) was determined by applying a threshold mask to determine the boundaries of the GFP-channel signal in each object (i.e. cell). The mean 488 signal of each object was then calculated. The average signal within the nucleus (termed “Nuclear DNA-PK”) was determined by creating a threshold mask based on the boundaries of the DAPI signal. This mask was then applied to

the companion 488 image and the mean 488 signal within this was then calculated. The mean signal intensity of each replicate was then averaged together to determine average signal intensity. The mean signal intensity from an average of 527 cells were used per condition per replicate.

2.7. Statistical analysis

All statistical analysis was performed using GraphPad Prism 8 (San Diego, CA). Effect of treatment and cell line was determined using a two-way ANOVA with Tukey's post-hoc test (Fig 3, 4 and 6E–H). Effect of cell line was determined using an unpaired two-tailed *t*-test (Fig. 6I–L). Significance was reached at $p < 0.05$. Significance is designated as $p < 0.05$ (*), $p \leq 0.0021$ (**), $p \leq 0.0002$ (***), $p \leq 0.0001$ (****). All quantified blots were normalized to a stain for total protein (REVERT; Licor)(Supplementary Fig. 4).

3. Results

FUS can be phosphorylated in cell culture following different drug treatments (Deng et al., 2014b; Monahan et al., 2017; Rhoads et al., 2018a). In particular, our lab discovered that the DNA-dependent protein kinase (DNA-PK) phosphorylates FUS in human-derived neurons and immortalized cell lines following double-strand DNA breaks (DSBs) induced by CLM (Deng et al., 2014b). However, the role of FUS phosphorylation in disease pathogenesis is unclear. Given this, we aimed to use primary mouse neurons as an *in vitro* model to investigate the function and disease mechanisms associated with FUS phosphorylation. Towards this aim, we first cultured primary cortical neurons from E18 C57BL/6 mice for 14 days then treated cultured neurons with increasing doses of CLM (1 to 1000 nM). Intriguingly, regardless of CLM concentration or length of treatment, we did not observe an increase in the molecular weight of FUS, an indication of FUS phosphorylation, in primary mouse neurons treated with CLM (Fig. 1A). Although we did not observe the appearance of p-FUS, we did detect phosphorylation of H2AX (p-H2AX), a marker of DNA damage, confirming CLM treatment caused DNA damage in mouse neurons (Podhorecka et al., 2010). In contrast, treatment of a human H4 neuroglioma cell line with CLM resulted in robust phosphorylation of FUS and H2AX (Fig. 1A). CLM treatment in mouse cells did lead to the production of multiple smaller fragments of FUS, which may indicate proteolytic cleavage, at the highest concentrations (100 and 1000 nM) and longest treatment times in primary mouse neurons (Fig. 1A, indicated by *). Interestingly, no smaller fragments of FUS were detected in multiple immortalized cell lines (HEK293T, SH-SY5Y or N2A) following CLM treatment, suggesting this cleavage may be unique to primary neuronal cells and should be examined in future studies (Supplemental Fig. 1). These data demonstrate that while CLM treatment causes DNA damage in mouse immortalized cells, it does not lead to phosphorylation of mouse FUS.

Because our previously published work exclusively utilized human-derived immortalized cell lines and primary neurons, we wondered whether CLM induced phosphorylation of FUS only occurred in human cells or if other primate cells exhibited the response. To investigate this, we asked if FUS phosphorylation occurred after CLM treatment in other primary cell lines derived from primates. First, we treated neural progenitor cells (NPCs) derived from

the rhesus macaque monkey with CLM. We observed a robust increase in p-FUS at 10 and 20 nM CLM in monkey NPCs (Fig. 1B). Neurons derived from monkey NPCs also phosphorylated FUS in response to CLM treatment (Fig. 1C). Lastly, we treated human iPSC-derived motor neurons (Fig. 1D) and primary human neurons (Fig. 1E) with increasing doses of CLM and saw a similar dose-dependent increase in p-FUS and p-H2AX signal. These data suggest that FUS phosphorylation following DSBs is a conserved phenomenon for multiple stages of primate neural development and does not occur in mouse-derived cells.

Previously we demonstrated that multiple human-derived immortalized cell lines can robustly phosphorylate FUS following CLM treatment (Deng et al., 2014b). Upon observing that primary murine cells did not phosphorylate FUS after CLM treatment, we asked if mouse-derived immortalized cell lines were able to phosphorylate FUS in response to CLM treatment. Unlike primary cells, immortalized cell lines are clonal, uniform, and can be grown indefinitely. As such, they offer a useful model for understanding cell-specific gene and protein dynamics (Kovalevich and Langford, 2013; Lendahl and McKay, 1990; Lin et al., 2014). We compared FUS phosphorylation following CLM treatment in HEK293T cells, a widely utilized human embryonic kidney cell line, to an immortalized mouse embryonic fibroblast (MEF) cell line. HEK293T cells showed a robust dose-dependent increase in FUS phosphorylation following CLM treatment indicated by a shift in molecular weight and co-immunoreactivity with a phospho-ATR/ATM Substrate Motif antibody, which detects the (pS/pT)QG motif that is phosphorylated by DNA-PK, ATR, and ATM (three closely related phosphoinositide 3-kinases) following DNA damage, as previously described (Blackford and Jackson, 2017; Deng et al., 2014b) (Fig. 2A). Alongside the appearance of the characteristic p-FUS top band, we observed a dose-dependent increase in p-H2AX signal, confirming that CLM treatment caused DNA damage (Fi 2A). In contrast, MEF cells exhibited no detectable FUS phosphorylation at any dose of CLM, despite having a robust p-H2AX signal (Fig. 2B). To determine if increased time may be necessary, we treated HEK293T and MEF cells in parallel with 10 nM CLM for 0.5 to 4 h and again found no detectable FUS phosphorylation signal in MEF cells (Fig. 2B). These data strongly suggest that MEF cells do not phosphorylate FUS following CLM induced double-strand DNA damage.

Given that FTD is a neurodegenerative disease, we examined the effect of CLM treatment on neuroblastoma cell lines, which have been used extensively as neuronal cell models of neurodegeneration (Xicoy et al., 2017). We observed a similar divergent response to CLM treatment in human SH-SY5Y neuroblastoma cells compared to mouse Neuro2A (N2A) neuroblastoma cells. SH-SY5Y cells showed a dose (Fig. 2C) and time (Fig. 2D) dependent phosphorylation of FUS following CLM treatment, similar to what we observed in other human-derived cell lines. In contrast, we did not detect any appreciable phosphorylation of FUS in the mouse-derived N2A cells in any condition tested (Fig 2C, D). Regardless of species, both human and mouse cell lines showed clear activation of p-H2AX response (Fig. 2C, D). Importantly, only human-derived HEK293T and SH-SY5Y cells had robust (pS/pT) QG immunoreactive bands following CLM treatment, suggesting there are differences in DNA damage response pathways in human versus mouse cells.

Next, we quantified the difference in phosphorylation response following CLM treatment between the human-derived SH-SY5Y cells and mouse-derived N2A cells (Fig. 3A). Given that the (pS/pT) QG residue antibody is not specific to only DNA-PK based phosphorylation, we also utilized a p-FUS antibody that specifically detects FUS phosphorylated at serine 30, one of the residues on FUS phosphorylated by DNA-PK following CLM treatment (Monahan et al., 2017; Murray et al., 2017; Rhoads et al., 2018a) (Fig. 3C, G). Additionally, we measured the amount of FUS present in the higher molecular weight band as in Deng et al. (2014b) (Fig. 3B, F). Using these two methods, we found that SH-SY5Y cells show a reproducible, dose-dependent and significant increase in both the total amount of p-FUS signal (Fig. 3B) and amount of p-FUS (Ser30) signal present (Fig. 3C). In agreement with our original results (Fig. 2), N2A cells showed no detectable p-FUS signal (Fig. 3B, C).

Previously, we reported that p-FUS accumulates in the cytoplasm of cells following CLM induced DSB (Deng et al., 2014b). Therefore, we tested if cytoplasmic FUS increased in N2A cells following CLM treatment (Fig. 3D). SH-SY5Y cells showed a significant increase in the total amount of FUS (Fig. 3E) and p-FUS (Fig. 3F–G) localized to the cytoplasmic fraction. In contrast, there was not a significant increase in FUS (Fig. 3E) or p-FUS (Fig. 3F–G) in the cytoplasm of mouse N2A cells following CLM treatment. Our data suggests that FUS is not phosphorylated, nor increased in the cytoplasm of mouse cells, following CLM induced DSB. In light of these findings, we aimed to determine why mouse cells did not phosphorylate FUS following CLM treatment.

First, we asked if mouse cells were capable of phosphorylating FUS under conditions that broadly increase protein phosphorylation. To do this, we treated cells with Calyculin A (Cal A), an inhibitor of the serine/threonine phosphatases PP1 and PP2A, which increases the appearance of the phosphorylated species of FUS (Deng et al., 2014b; Ishihara et al., 1989). Given the wide breath of targets for PP1 and PP2A and the ~50 residues spread throughout the primary amino acid sequence of FUS that can be phosphorylated, the phosphorylated species of FUS triggered by Cal A may not be same as the phosphorylated FUS caused by DNA damage mechanisms (Rhoads et al., 2018b). Therefore, we aimed to confirm whether mouse FUS could be phosphorylated independently of DNA damage response pathways. Increasing doses of Cal A in mouse N2A cells caused the appearance of a slightly higher molecular weight FUS band, which could be due to phosphorylation (Fig. 4A). However, there was little to no overlap between the p-FUS band and signal from the (pS/pT)QG antibody suggesting Cal A treatment may lead to FUS phosphorylation at non-DNA-PK target residues. Therefore, we tested whether phosphorylation of the DNA-PK target residue Ser30 could be detected following Cal A treatment (Fig. 4B). SH-SY5Y showed a significant increase in p-FUS signal following Cal A treatment ($p = 0.0491$; Fig. 4C). Although we were able to detect a faint p-FUS (Ser30) band in both SH-SY5Y and N2A cells following Cal A treatment, the N2A treated cells did not have a significantly different p-FUS signal compared to controls ($p = 0.3439$; Fig. 4C). These data suggests that although FUS can be phosphorylated in mouse cells, this response is not robust following Cal A treatment and the overall extent of phosphorylation appears much lower than in primate-derived cell lines (Supplemental Fig. 2C). Next, we asked if staurosporine, a broad kinase inhibitor, inducer of apoptosis, and an activator of DNA-PK, could induce p-FUS in mouse

cells (Chakravarthy et al., 1999; Karaman et al., 2008). We focused on staurosporine because it was the original chemical we first used to discover FUS phosphorylation and a known inducer p-H2AX (Deng et al., 2014b; Solier and Pommier, 2009). Treatment of mouse N2A cells with 1 μM staurosporine for up to four hours did not cause phosphorylation of FUS (Fig. 4B). However, staurosporine did induce apoptosis and DNA damage at this dose as confirmed by the appearance of cleaved Poly (ADP-ribose) polymerase (PARP) and an increase in p-H2AX signal (Fig. 4B). In contrast, treatment of SH-SY5Y cells with 1 or 2 μM staurosporine induced reliable FUS phosphorylation detected by a band shift (Supplemental Fig. 2A) and p-FUS (Ser30) signal (Fig. 4E). This difference was quantified showing that p-FUS (Ser30) was significantly higher in SH-SY5Y following staurosporine treatment compared to controls ($p = 0.0145$) or N2A cells (Fig. 4G). Taken together, these data suggest that while mouse cells are capable of phosphorylating FUS, DSBs may not cause robust phosphorylation of FUS. Therefore, we conclude that the DNA damage response triggered by double-strand breaks does not initiate FUS phosphorylation in mouse-derived cells.

Since mouse cells did not phosphorylate FUS following either CLM or staurosporine induced DNA-damage, we reasoned that either 1) mouse cells lack the required signaling cascade to activate DNA-PK or 2) mouse FUS does not contain the correct amino acid residues to be phosphorylated after DNA damage. While FUS can be phosphorylated at many sites, double-strand DNA damage induces phosphorylation at 12 specific serine or threonine residues spread throughout the N-terminus of the protein (Gardiner et al., 2008; Monahan et al., 2017). This N-terminal region, deemed the low-complexity domain, contains a SYGQ-rich and a glycine-rich domain. Human and mouse FUS are very similar and share ~95% amino acid identity over the entire protein (Fig 5A). However, there are 26 amino acid differences and 25 of those exist in the low complexity domain of the N-terminus of the protein (Fig. 5A). Therefore, we asked if the inability of mouse cells to phosphorylate FUS following CLM treatment could be due to these sequence differences. We tested this by expressing GFP-tagged mouse FUS (GFP-mFUS) in human HEK293T cells and GFP-tagged human FUS (GFP-hFUS) in mouse N2A cells. Then, we treated cells with CLM to induce FUS phosphorylation. In HEK293T cells, both endogenous human FUS and exogenously expressed GFP-mFUS were phosphorylated (Fig. 5B). FUS phosphorylation was confirmed by an increase in molecular weight and the appearance of a p-FUS signal using the antibody specific to FUS phosphorylated at Ser30, a residue that is present in both human and mouse FUS. In contrast, we did not detect phosphorylation of endogenous mouse FUS or exogenous GFP-hFUS in N2A cells (Fig. 5B). These data reveal that while mouse FUS can be robustly phosphorylated in human cells, mouse cells do not phosphorylate human FUS, suggesting the pathways necessary to phosphorylate FUS following DNA damage in mouse cells are not present, or as active, compared to primate cells.

Given that mouse FUS can be modestly phosphorylated, we next asked whether some aspect of the pathway leading to FUS phosphorylation is different between human and mouse cells. We focused on DNA-PK because DNA-PK phosphorylates FUS following CLM induced double-strand DNA damage (Deng et al., 2014b). Moreover, previous reports suggest that the concentration of DNA-PK is lower in mouse cells compared to human cells (Finnie et al., 1995; Lees-Miller et al., 1992). Therefore, we first aimed to determine if N2A cells have

a lower concentration of total DNA-PK compared to SH-SY5Y cells. We used a DNA-PK antibody that can detect both human and mouse DNA-PK species (Supplemental Fig. 3). Immunoblotting of cell lysates revealed that while SH-SY5Y and N2A cells express similar levels of FUS protein, SH-SY5Y cells express much higher levels of total DNA-PK compared to N2A cells (Fig. 6A). Treatment of either cell line with CLM did not change the total levels of DNA-PK (Fig. 6A). We next asked if mouse DNA-PK was properly activated following CLM treatment. DNA-PK's catalytic activity is dependent on phosphorylation of residue S2056 in humans, S2053 in mice, making phosphorylation of S2056/3 a widely used marker of DNA-PK activity (Chan et al., 2002; Chen et al., 2005; Jiang et al., 2019; Merkle et al., 2002). It should be noted that the antibody used to detect phosphorylated DNA-PK has been validated to cross-react with the mouse S2053 site by immunofluorescence allowing us to use the same antibody in our comparison (Roch et al., 2019). Treatment of SH-SY5Y cells with CLM at 10 and 40 nM caused activation of DNA-PK, as detected by the appearance of phosphorylated DNA-PK (p-DNA-PK at S2056/3). In contrast, we did not detect phosphorylation of DNA-PK or FUS in N2A cells via immunoblot at any dose of CLM tested (Fig. 6B).

Next, we used immunofluorescence to examine the subcellular localization of DNA-PK in SH-SY5Y and N2A cells using a total DNA-PK antibody that recognizes both mouse and human DNA-PK. The overall fluorescent intensity for DNA-PK was significantly higher in SH-SY5Y compared to N2A cells, confirming our western blot results (Fig. 6C, E). Intriguingly, the DNA-PK signal appeared more diffuse throughout the cytoplasm and the nucleus of N2A cells, while DNA-PK immunoreactivity in SH-SY5Y cells was more predominant in the nucleus (Fig. 6C). Quantification of immunofluorescence confirmed the presence of significantly more DNA-PK in the nucleus of SH-SY5Y compared to N2A regardless of treatment (Fig. 6F). Furthermore, CLM treatment for either SH-SY5Y or N2A cells did not change the cellular localization of DNA-PK (Fig. 6F). In line with this, the proportion of DNA-PK signal remained unchanged (around ~1) between control and treatment for both SH-SY5Y and N2A cells when examining the whole cell (Fig. 6I) and nucleus (Fig. 6J).

We next asked if DNA-PK was activated following CLM treatment in mouse and human cells. We treated SH-SY5Y and N2A cells with CLM (20 nM) and measured the amount of phosphorylated DNA-PK S2056 (p-DNA-PK) signal. In untreated control cells, p-DNA-PK staining in both N2A and SH-SY5Y cells was weak and diffuse throughout the nucleus and cytoplasm (Fig. 6D). As expected, SH-SY5Y cells had robust DNA-PK activation following CLM treatment, as measured by phosphorylation of the S2056 (S2053 for N2A cells) residue on DNA-PK (Fig. 6D, G). Unexpectedly, N2A cells exhibited an increase in p-DNA-PK whole cell signal (Fig. 6G) and nuclear signal (Fig. 6H) following CLM treatment. However, the proportion of p-DNA-PK signal was significantly higher in SH-SY5Y compared to N2A for both the whole cell ($p = 0.0442$; Fig. 6K) and the nucleus ($p = 0.0389$; Fig. 6L). Overall, this data suggests that while mouse cells are capable of activating DNA-PK in response to CLM, the amount of p-DNA-PK available is significantly lower in mouse cells compared to human cells. Taken together, these data support the idea that CLM treatment of mouse cells does not lead to FUS phosphorylation due to differences in the DNA-PK mediated DNA damage and repair response in mice versus human cells.

4. Discussion

Our previous work found that both primary and immortalized human cells robustly phosphorylate FUS in response to DSBs and that this response is mediated by DNA-PK activation. Furthermore, we found that CLM treatment in particular is a potent and useful chemical trigger of FUS phosphorylation (Deng et al., 2014b). Previously, we and others have shown that CLM-induced FUS phosphorylation can be detected through 1) a band shift, or more precisely, an increase in the apparent molecular weight of FUS migrating on a SDS/PAGE gel due to phosphorylation and 2) overlap of the higher-molecular weight FUS with a phospho ATM/ATR substrate motif antibody that specifically detects (pS/pT) QG phosphorylation, the preferred phosphorylation site of DNA-PK (Deng et al., 2014b; Kim et al., 1999; Rhoads et al., 2018a). In this current work, we utilized both detection methods and found that neither primary nor immortalized mouse-derived cells phosphorylate FUS following CLM treatment. Although we were unable to detect a band shift, or overlap in FUS signal with the p-S/p-T antibody in mouse derived cells, we did see the appearance of p-H2AX, a crucial regulator of the DSB response and a known target of DNA-PK, verifying that CLM treatment was adequate to induce DNA damage and repair processes (An et al., 2010).

CLM is not the only known chemical that induces FUS phosphorylation. Our previous work showed that treatment of human cells with Cal A and staurosporine caused FUS phosphorylation. Cal A is an potent inhibitor of the PP1 and PP2A protein phosphatases and Cal A treatment is known to cause an increase in global protein phosphorylation by blocking de-phosphorylation (Chartier et al., 1991). Surprisingly though, Cal A only induced a modest amount of FUS phosphorylation in mouse cells suggesting mouse cells achieve less FUS phosphorylation than human cells. At the protein sequence level, mice and human FUS are nearly identical and contain almost all the same phosphorylation target residues. Therefore, future studies should explore whether this difference in basal phosphorylation is due to 1) differences in mouse PP1 and PP2A protein phosphatase activity and 2) whether other the post-translational modifications such as acetylation or ubiquitination are also different between mouse and human FUS.

Staurosporine is a cell permeable broad protein kinase inhibitor previously shown to activate DNA-PK (Chakravarthy et al., 1999). Treatment with staurosporine did not cause FUS phosphorylation or the appearance of p-H2AX in mouse cells. Interestingly, human cells treated with staurosporine show robust p-H2AX activation (Supplemental Fig. 2B). Histone H2AX is a substrate of the phosphoinositide 3-kinase-related protein kinases, DNA-PK, ATM, and ATR, which phosphorylate H2AX at residue Ser139 in response to DSBs (An et al., 2010; Podhorecka et al., 2010). p-H2AX is thought to act as a docking site that recruits repair factors to the site of repair (Podhorecka et al., 2010). In line with this, evidence suggests that reduced phosphorylation of H2AX leads to improper DSB repair and genomic instability (Celeste et al., 2003; Revet et al., 2011). As such, the lack of p-H2AX and p-FUS activation suggests that mouse cells have a divergent response to staurosporine induced DNA-PK activation. Taken together, our data demonstrate that mouse cells exhibit divergent FUS phosphorylation when compared to human cells.

Next, we investigated why mouse cells exhibit this divergent response to DSB. As stated, CLM is a potent inducer of DSBs (Dedon et al., 1993; Elmroth et al., 2003). DSBs are repaired in mammalian cells through either homologous recombination or non-homologous end-joining (NHEJ) (Bohgaki et al., 2010). DNA-PK is thought to be both a sensor and a transducer of DNA-damage and autophosphorylation of DNA-PK at S2056 (S2053 for mice) after DNA-damage is required for efficient NHEJ (Chan et al., 2002; Chen et al., 2005; Jiang et al., 2019; Merkle et al., 2002). Furthermore, activation of DNA-PK leads to the recruitment and phosphorylation of other DNA-repair proteins (Burma and Chen, 2004). Therefore, improper activation of DNA-PK would inhibit the DNA damage response. We showed that mouse cells do not phosphorylated FUS in response to two DNA-PK activators, CLM and staurosporine. Furthermore, our data show that mouse FUS can be phosphorylated when expressed in human cells, suggesting the issue lies in the response of mouse cells to DNA damage and not mouse FUS itself. Together, these data suggests that the divergent response is due to mouse DNA-PK not being properly activated.

Previously, it has been reported that DNA-PK activity is much lower in mouse than in human tissue (Finnie et al., 1995; Lees-Miller et al., 1992). We recapitulated this finding and found that DNA-PK expression is much lower in mouse cells compared to human cells. Further, CLM treatment causes decreased activation of DNA-PK in mouse cells compared to human cells. Adequate DNA-PK activity and expression is necessary for proper DSB repair (Okayasu et al., 2000). As such, decreased DNA-PK expression in mice would affect DSB repair. DNA-PK expression and activation are not the only differences between mice and human DNA repair. Specifically, it is known that longer-lived species such as humans have higher expression of DNA repair genes and pathways (MacRae et al., 2015; Waterston et al., 2002). Additionally, multiple aspects of the DNA damage response and DNA repair pathways are significantly different between human and mouse neurons (Martin and Chang, 2018). As such, extensive prior data demonstrate that mouse cells do not recapitulate all aspects of DNA damage response and repair pathways that occur in human derived cell models.

Given these reported differences in DNA repair, we show that DNA-PK expression and activation is lower in mouse-derived cells, but the cause is unclear. DNA-PK activation is a complex process where multiple proteins and responses can lead to autophosphorylation and activation of DNA-PK (Burma and Chen, 2004). Our work and others show that mouse DNA-PK is sufficiently activated enough by CLM induced DSBs to cause phosphorylation of H2AX (p-H2AX) (Audebert et al., 2004; Deng et al., 2014b; Podhorecka et al., 2010). In addition, we find a CLM dependent increase in the immunostaining of p-DNA-PK in mouse cells. Both of these lines of evidence suggest DNA-PK is activated to some extent, yet this still does not lead to phosphorylation of FUS. It is possible that activation, or inhibition, of another protein is required to enable DNA-PK mediated phosphorylation of FUS. One possibility is PARP1, a known binding partner of FUS (Mastrocola et al., 2013). Recent work shows that PARP1 directs FUS to sites of DNA damage (Rulten et al., 2013; Singatulina et al., 2019). Therefore, ineffective PARP1 activation or recruitment to sites of DSBs might cause improper trafficking of FUS to these sites preventing the interaction of FUS and DNA-PK. In support of this idea, PARP1 inhibition has been shown to cause increased p-H2AX, a characteristic difference we noticed between mouse and human cells

following CLM treatment (Audebert et al., 2004). This suggests PARP1 may not be activated in mouse cells following CLM treatment. Future studies should examine the PARP1-FUS-DNA-PK interaction complex further.

The species-specific difference in FUS phosphorylation we uncovered is also relevant for attempts to model FUS and FET pathology in mice. Broadly speaking, mouse models have yielded valuable insights into the pathogenesis of FTD and ALS (Ahmed et al., 2017; Van Damme et al., 2017). However, these models also have limitations, and often do not fully recapitulate all aspects of FTD or ALS (Dawson et al., 2018; Perrin, 2014). Most relevant to this work is the lack of a mouse model that recapitulates FTLD with FET pathology. One roadblock to this goal is that the specific genetic or environmental cause of FTLD-FET is still unclear. For example, although FUS is hypomethylated in FTLD-FET inclusions, mutations in protein N-arginine methyltransferase genes are not found in FTLD, leaving the cause unknown (Dormann et al., 2012; Ravenscroft et al., 2013). Recently, additional heterogeneous nuclear ribonucleoproteins (hnRNP P and Q) were found to co-aggregate with FUS, suggesting that wide-spread dysfunction of RNA metabolism contributes to the development of FTLD-FET (Gami-Patel et al., 2016; Gittings et al., 2019; Lagier-Tourenne et al., 2010; Ravenscroft et al., 2013). More research is needed to understand the similarities, differences, and cause(s) of the various FTLD sub-types. As such, our study suggests that the fundamental differences in DNA damage response between mice and humans should be considered in efforts to model FTD pathology, as well as understand pathogenesis.

In summary, we have uncovered a distinct inability of mouse cells to phosphorylate FUS following DNA damage. Even in the presence of DSBs and p-H2AX, mouse cells do not phosphorylate FUS. Our data suggest that decreased levels and activity of DNA-PK are an important factor why FUS is not phosphorylated in mouse cells following CLM treatment. We cannot rule out that impairments in other components involved in the DNA damage response pathway also contribute to the lack of FUS phosphorylation we observe in multiple mouse cell lines. Future studies should examine in more detail the differential response of mouse cells to CLM compared to human cells.

Supplementary Material

Refer to Web version on PubMed Central for supplementary material.

Acknowledgements

We would like to thank the members of the Kukar lab and the Emory Center for Neurodegenerative Disease for useful discussions and suggestions about this work. We also thank Dr. Frank Shewmaker and his lab for generously providing p-FUS specific antibodies.

Funding sources

This work was supported by the National Institutes of Health (NIH)/NINDS grants (R01 NS093362, R01 NS105971), a New Vision Research Investigator Award, an Emory Alzheimer's Disease Center Pilot Grant P50AG025688, the Alzheimer's Drug Discovery Foundation and the Association for Frontotemporal Degeneration (ADDF/AFTD), the Bluefield Project to Cure Frontotemporal Dementia, and the BrightFocus Foundation to Thomas Kukar.

Abbreviations:

CLM	Calicheamicin γ1
Cal A	Calyculin A

References

Ahmed RM, et al., 2017. Mouse models of frontotemporal dementia: a comparison of phenotypes with clinical symptomatology. Neurosci. Biobehav. Rev 74, 126–138. [PubMed: 28088537]

An J, et al., 2010. DNA-PKcs plays a dominant role in the regulation of H2AX phosphorylation in response to DNA damage and cell cycle progression. BMC Mol. Biol 11, 18. [PubMed: 20205745]

Andersson MK, et al., 2008. The multifunctional FUS, EWS and TAF15 proto-onco-proteins show cell type-specific expression patterns and involvement in cell spreading and stress response. BMC Cell Biol. 9, 37. [PubMed: 18620564]

Audebert M, et al., 2004. Involvement of poly(ADP-ribose) polymerase-1 and XRCC1/DNA ligase III in an alternative route for DNA double-strand breaks rejoining. J. Biol. Chem 279, 55117–55126. [PubMed: 15498778]

Bahia VS, et al., 2013. Neuropathology of frontotemporal lobar degeneration: a review. Dement Neuropsychol. 7, 19–26. [PubMed: 29213815]

Bang J, et al., 2015. Frontotemporal dementia. Lancet (Lond. Eng.) 386, 1672–1682.

Blackford AN, Jackson SP, 2017. ATM, ATR, and DNA-PK: the trinity at the heart of the DNA damage response. Mol. Cell 66, 801–817. [PubMed: 28622525]

Bohgaki T, et al., 2010. DNA double-strand break signaling and human disorders. Genome Integr. 1, 15. [PubMed: 21054854]

Bowden HA, Dormann D, 2016. Altered mRNP granule dynamics in FTLD pathogenesis. J. Neurochem 138 (Suppl. 1), 112–133. [PubMed: 26938019]

Boxer AL, et al., 2020. New directions in clinical trials for frontotemporal lobar degeneration: methods and outcome measures. Alzheimers Dement. 16, 131–143. [PubMed: 31668596]

Broustal 0, et al., 2010. FUS mutations in frontotemporal lobar degeneration with amyotrophic lateral sclerosis. J. Alzheimers Dis 22, 765–769. [PubMed: 21158017]

Burma S, Chen DJ, 2004. Role of DNA-PK in the cellular response to DNA double-strand breaks. DNA Repair 3, 909–918. [PubMed: 15279776]

Carter RL, et al., 2014. Reversal of cellular phenotypes in neural cells derived from Huntington's disease monkey-induced pluripotent stem cells. Stem Cell Rep. 3, 585–593.

Celeste A, et al., 2003. H2AX haploinsufficiency modifies genomic stability and tumor susceptibility. Cell 114, 371–383. [PubMed: 12914701]

Chakravarthy BR, et al., 1999. Activation of DNA-dependent protein kinase may play a role in apoptosis of human neuroblastoma cells. J. Neurochem 72, 933–942. [PubMed: 10037464]

Chan DW, et al., 2002. Autophosphorylation of the DNA-dependent protein kinase catalytic subunit is required for rejoining of DNA double-strand breaks. Genes Dev. 16, 2333–2338. [PubMed: 12231622]

Chartier L, et al., 1991. Calyculin-a increases the level of protein phosphorylation and changes the shape of 3T3 fibroblasts. Cell Motil. Cytoskeleton 18, 26–40. [PubMed: 1848484]

Chen BPC, et al., 2005. Cell cycle dependence of DNA-dependent protein kinase phosphorylation in response to DNA double strand breaks. J. Biol. Chem 280, 14709–14715. [PubMed: 15677476]

Cho IK, et al., 2019a. Combination of stem cell and gene therapy ameliorates symptoms in Huntington's disease mice. NPJ Regener. Med 4, 7.

Cho IK, et al., 2019b. Amelioration of Huntington's disease phenotype in astrocytes derived from iPSC-derived neural progenitor cells of Huntington's disease monkeys. PLoS One 14, e0214156. [PubMed: 30897183]

Darovic S, et al., 2015. Phosphorylation of C-terminal tyrosine residue 526 in FUS impairs its nuclear import. J. Cell Sci 128, 4151–4159. [PubMed: 26403203]

Dawson TM, et al., 2018. Animal models of neurodegenerative diseases. Nat. Neurosci 21, 1370–1379. [PubMed: 30250265]

De Santis R, et al., 2017. FUS Mutant Human Motoneurons Display Altered Transcriptome and microRNA Pathways with Implications for ALS Pathogenesis. (Stem cell reports).

Dedon PC, et al., 1993. Exclusive production of bistranded DNA damage by calicheamicin. Biochemistry 32, 3617–3622. [PubMed: 8466904]

Deng H, et al., 2014a. The role of FUS gene variants in neurodegenerative diseases. Nat. Rev. Neurol 10, 337–348. [PubMed: 24840975]

Deng Q, et al., 2014b. FUS is phosphorylated by DNA-PK and accumulates in the cytoplasm after DNA damage. J. Neurosci 34, 7802–7813. [PubMed: 24899704]

Dormann D, et al., 2012. Arginine methylation next to the PY-NLS modulates Transportin binding and nuclear import of FUS. EMBO J. 31, 4258–4275. [PubMed: 22968170]

Elmroth K, et al., 2003. Cleavage of cellular DNA by calicheamicin gammal. DNA Repair 2, 363–374. [PubMed: 12606118]

Finnie NJ, et al., 1995. DNA-dependent protein kinase activity is absent in xrs-6 cells: implications for site-specific recombination and DNA double-strand break repair. Proc. Natl. Acad. Sci 92, 320–324. [PubMed: 7816841]

Fujii R, et al., 2005. The RNA binding protein TLS is translocated to dendritic spines by mGluR5 activation and regulates spine morphology. Curr. Biol 15, 587–593. [PubMed: 15797031]

Gami-Patel P, et al., 2016. The presence of heterogeneous nuclear ribonucleoproteins in frontotemporal lobar degeneration with FUS-positive inclusions. Neurobiol. Aging 46, 192–203. [PubMed: 27500866]

Gardiner M, et al., 2008. Identification and characterization of FUS/TLS as a new target of ATM. Biochem. J 415, 297–307. [PubMed: 18620545]

Gittings LM, et al., 2019. Heterogeneous nuclear ribonucleoproteins R and Q accumulate in pathological inclusions in FTLD-FUS. Acta Neuropathol. Commun 7, 13–18. [PubMed: 30704515]

Higelin J, et al., 2016. FUS mislocalization and vulnerability to DNA damage in ALS patients derived hiPSCs and aging motoneurons. Front. Cell. Neurosci 10, 290. [PubMed: 28082870]

Hodges JR, et al., 2003. Survival in frontotemporal dementia. Neurology 61, 349–354. [PubMed: 12913196]

Holler CJ, et al., 2017. Intracellular proteolysis of Progranulin generates stable, lysosomal Granulins that are Haploinsufficient in patients with frontotemporal dementia caused by GRN mutations. eNeuro 4.

Ishihara H, et al., 1989. Calyculin a and okadaic acid: inhibitors of protein phosphatase activity. Biochem. Biophys. Res. Commun 159, 871–877. [PubMed: 2539153]

Jiang W, et al., 2019. Phosphorylation at S2053 in murine (S2056 in human) DNA-PKcs is dispensable for lymphocyte development and class switch recombination. J. Immunol 203, 178–187. [PubMed: 31101667]

Kamelgarn M, et al., 2016. Proteomic analysis of FUS interacting proteins provides insights into FUS function and its role in ALS. Biochim. Biophys. Acta 1862, 2004–2014. [PubMed: 27460707]

Karaman MW, et al., 2008. A quantitative analysis of kinase inhibitor selectivity. Nat. Biotechnol 26, 127–132. [PubMed: 18183025]

Kim ST, et al., 1999. Substrate specificities and identification of putative substrates of ATM kinase family members. J. Biol. Chem 274, 37538–37543. [PubMed: 10608806]

Knopman DS, Roberts RO, 2011. Estimating the number of persons with frontotemporal lobar degeneration in the US population. J. Mol. Neurosci 45, 330–335. [PubMed: 21584654]

Kovalevich J, Langford D, 2013. Considerations for the use of SH-SY5Y neuroblastoma cells in neurobiology. Methods Mol. Biol. (Clifton, NJ) 1078, 9–21.

Kwiatkowski TJ, et al., 2009. Mutations in the FUS/TLS gene on chromosome 16 cause familial amyotrophic lateral sclerosis. Science (New York, N.Y.) 323, 1205–1208.

Lagier-Tourenne C, et al., 2010. TDP-43 and FUS/TLS: emerging roles in RNA processing and neurodegeneration. Hum. Mol. Genet 19, R46–R64. [PubMed: 20400460]

Lees-Miller SP, et al., 1992. Human DNA-activated protein kinase phosphorylates serines 15 and 37 in the amino-terminal transactivation domain of human p53. Mol. Cell. Biol 12, 5041–5049. [PubMed: 1406679]

Lendahl U, McKay RD, 1990. The use of cell lines in neurobiology. Trends Neurosci. 13, 132–137. [PubMed: 1692169]

Lin Y-C, et al., 2014. Genome dynamics of the human embryonic kidney 293 lineage in response to cell biology manipulations. Nat. Commun 5, 4767. [PubMed: 25182477]

Mackenzie IRA, et al., 2009. Nomenclature for neuropathologic subtypes of frontotemporal lobar degeneration: consensus recommendations. Acta Neuropathol. 117, 15–18. [PubMed: 19015862]

Mackenzie IRA, et al., 2010. Nomenclature and nosology for neuropathologic subtypes of frontotemporal lobar degeneration: an update. Acta Neuropathol. 119, 1–4. [PubMed: 19924424]

MacRae SL, et al., 2015. DNA repair in species with extreme lifespan differences. Aging 7, 1171–1184. [PubMed: 26729707]

Martin LJ, Chang Q, 2018. DNA damage response and repair, DNA methylation, and cell death in human neurons and experimental animal neurons are different. J. Neuropathol. Exp. Neurol 77, 636–655. [PubMed: 29788379]

Mastrocola AS, et al., 2013. The RNA-binding protein fused in sarcoma (FUS) functions downstream of poly(ADP-ribose) polymerase (PARP) in response to DNA damage. J. Biol. Chem 288, 24731–24741. [PubMed: 23833192]

Merkle D, et al., 2002. The DNA-dependent protein kinase interacts with DNA to form a protein-DNA complex that is disrupted by phosphorylation. Biochemistry 41, 12706–12714. [PubMed: 12379113]

Mitchell JC, et al., 2012. Overexpression of human wild-type FUS causes progressive motor neuron degeneration in an age- and dose-dependent fashion. Acta Neuropathol. 125, 273–288. [PubMed: 22961620]

Monahan Z, et al., 2017. Phosphorylation of the FUS low-complexity domain disrupts phase separation, aggregation, and toxicity. EMBO J. 36, 2951–2967 e201696394. [PubMed: 28790177]

Murray DT, et al., 2017. Structure of FUS protein fibrils and its relevance to self-assembly and phase separation of low-complexity domains. Cell 171, 615–627. [PubMed: 28942918]

Naumann M, et al., 2018. Impaired DNA damage response signaling by FUS-NLS mutations leads to neurodegeneration and FUS aggregate formation. Nat. Commun 9, 1208. [PubMed: 29572438]

Neumann M, Mackenzie IRA, 2019. Review: neuropathology of non-tau frontotemporal lobar degeneration. Neuropathol. Appl. Neurobiol 45, 19–40. [PubMed: 30357887]

Neumann M, et al., 2009. A new subtype of frontotemporal lobar degeneration with FUS pathology. Brain J. Neurol 132, 2922–2931.

Niu C, et al., 2012. FUS-NLS/Transportin 1 complex structure provides insights into the nuclear targeting mechanism of FUS and the implications in ALS. PLoS One 7, e47056. [PubMed: 23056579]

Okayasu R, et al., 2000. A deficiency in DNA repair and DNA-PKcs expression in the radiosensitive BALB/c mouse. Cancer Res. 60, 4342–4345. [PubMed: 10969773]

Perrin S, 2014. Preclinical research: make mouse studies work. Nature 507, 423–425. [PubMed: 24678540]

Podhorecka M, et al., 2010. H2AX phosphorylation: its role in DNA damage response and Cancer therapy. J. Nucleic Acids 2010.

Ravenscroft TA, et al., 2013. Mutations in protein N-arginine methyltransferases are not the cause of FTLD-FUS. Neurobiol. Aging 34 2235.e11–3.

Renton AE, et al., 2014. State of play in amyotrophic lateral sclerosis genetics. Nat. Neurosci 17, 17–23. [PubMed: 24369373]

Revet I, et al., 2011. Functional relevance of the histone gammaH2Ax in the response to DNA damaging agents. Proc. Natl. Acad. Sci. U. S. A 108, 8663–8667. [PubMed: 21555580]

Rhoads SN, et al., 2018a. The prionlike domain of FUS is multiphosphorylated following DNA damage without altering nuclear localization. Mol. Biol. Cell 29, 1786–1797. [PubMed: 29897835]

Rhoads SN, et al., 2018b. The role of post-translational modifications on prion-like aggregation and liquid-phase separation of FUS. Int. J. Mol. Sci 19.

Roch B, et al., 2019. Cernunnos/X1f deficiency results in suboptimal V(D)J recombination and impaired lymphoid development in mice. Front. Immunol 10, 443. [PubMed: 30923523]

Rohrer JD, et al., 2009. The heritability and genetics of frontotemporal lobar degeneration. Neurology 73, 1451–1456. [PubMed: 19884572]

Rulten SL, et al., 2013. PARP-1 dependent recruitment of the amyotrophic lateral sclerosis-associated protein FUS/TLS to sites of oxidative DNA damage. Nucleic Acids Res. 42, 307–314. [PubMed: 24049082]

Sala C, et al., 2000. Developmentally regulated NMDA receptor-dependent dephosphorylation of cAMP response element-binding protein (CREB) in hippocampal neurons. J. Neurosci 20, 3529–3536. [PubMed: 10804193]

Sama R, et al., 2013. FUS/TLS assembles into stress granules and is a prosurvival factor during hyperosmolar stress. Wiley Online Library 228, 2222–2231.

Sama RR, et al., 2014. Functions of FUS/TLS from DNA repair to stress response: implications for ALS. ASN Neuro 6.

Scaramuzzino C, et al., 2013. Protein arginine methyltransferase 1 and 8 interact with FUS to modify its sub-cellular distribution and toxicity in vitro and in vivo. PLoS One 8, e61576. [PubMed: 23620769]

Scekic-Zahirovic J, et al., 2016. Toxic gain of function from mutant FUS protein is crucial to trigger cell autonomous motor neuron loss. EMBO J. 35, 1077–1097. [PubMed: 26951610]

Schindelin J, et al., 2012. Fiji: an open-source platform for biological-image analysis. Nat. Methods 9, 676–682. [PubMed: 22743772]

Schneider CA, et al., 2012. NIH image to ImageJ: 25 years of image analysis. Nat. Methods 9, 671–675. [PubMed: 22930834]

Schwartz JC, et al., 2012. FUS binds the CTD of RNA polymerase II and regulates its phosphorylation at Ser2. Genes Dev. 26, 2690–2695. [PubMed: 23249733]

Shelkovnikova TA, et al., 2013. Recruitment into stress granules prevents irreversible aggregation of FUS protein mislocalized to the cytoplasm. Cell Cycle 12, 3194–3202. [PubMed: 24013423]

Sievers F, et al., 2011. Fast, scalable generation of high-quality protein multiple sequence alignments using Clustal omega. Mol. Syst. Biol 7, 539. [PubMed: 21988835]

Singatulina AS, et al., 2019. PARP-1 activation directs FUS to DNA damage sites to form PARG-reversible compartments enriched in damaged DNA. Cell Rep. 27, 1809–1821 e5. [PubMed: 31067465]

Snowden JS, et al., 2011. The most common type of FTLD-FUS (aFTLD-U) is associated with a distinct clinical form of frontotemporal dementia but is not related to mutations in the FUS gene. Acta Neuropathol. 122, 99–110. [PubMed: 21424531]

Solier S, Pommier Y, 2009. The apoptotic ring: a novel entity with phosphorylated histones H2AX and H2B and activated DNA damage response kinases. Cell Cycle 8, 1853–1859. [PubMed: 19448405]

Svetoni F, et al., 2016. Role of FET proteins in neurodegenerative disorders. RNA Biol. 13, 1089–1102. [PubMed: 27415968]

Tan AY, et al., 2012. TLS/FUS (translocated in liposarcoma/fused in sarcoma) regulates target gene transcription via single-stranded DNA response elements. Proc. Natl. Acad. Sci 109, 6030–6035. [PubMed: 22460799]

Van Damme P, et al., 2017. Modelling amyotrophic lateral sclerosis: progress and possibilities. Dis. Model. Mech 10, 537–549. [PubMed: 28468939]

Vance C, et al., 2009. Mutations in FUS, an RNA processing protein, cause familial amyotrophic lateral sclerosis type 6. Science (New York, N.Y.) 323, 1208–1211.

Verbeeck C, et al., 2012. Expression of fused in sarcoma mutations in mice recapitulates the neuropathology of FUS proteinopathies and provides insight into disease pathogenesis. Mol. Neurodegener 7, 53. [PubMed: 23046583]

Vieira RT, et al., 2013. Epidemiology of early-onset dementia: a review of the literature. Clin. Pract. Epidemiol. Ment. Health 9, 88–95. [PubMed: 23878613]

Waterston RH, et al., 2002. Initial sequencing and comparative analysis of the mouse genome. Nature 420, 520–562. [PubMed: 12466850]

Xicoy H, et al., 2017. The SH-SY5Y cell line in Parkinson's disease research: a systematic review. Mol. Neurodegener 12, 10–11. [PubMed: 28118852]

Yang L, et al., 2014. Self-assembled FUS binds active chromatin and regulates gene transcription. Proc. Natl. Acad. Sci. U. S. A 111, 17809–17814. [PubMed: 25453086]

Zinszner H, et al., 1997. TLS (FUS) binds RNA in vivo and engages in nucleo-cytoplasmic shuttling. J. Cell Sci 110 (Pt 15), 1741–1750. [PubMed: 9264461]

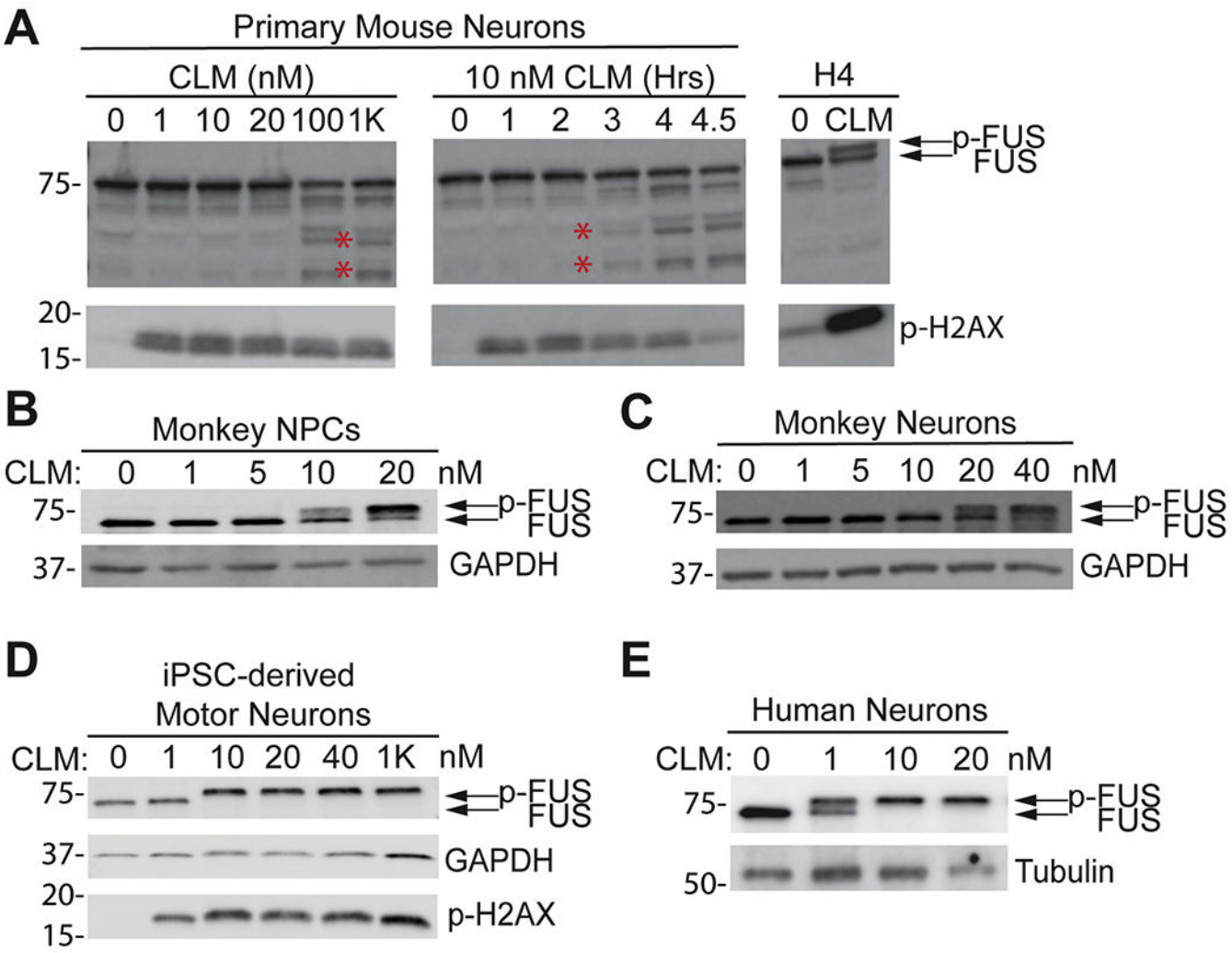

Fig. 1.

Calicheamicin γ-1 (CLM) treatment induces FUS phosphorylation in human and non-human primate neurons, but not primary mouse neurons. (A) Primary mouse neurons were treated either with increasing doses of CLM (nM) for 2 h (left) or with 10 nM CLM for increasing times (0 to 4.5 h) (right). In comparison, human H4 neuroglioma cells were treated with either DMSO (vehicle) or 10 nM CLM for 3 h. RIPA extracted whole cell lysates were analyzed by immunoblotting using indicated cellular markers. A positive p-H2AX signal indicates the occurrence of double strand DNA damage in mouse and human cells. (*) indicates potential FUS cleavage products following CLM treatment. In contrast, all human and non-human primate (monkey) derived neuronal models display the characteristic dose dependent phosphorylation of FUS following CLM treatment. (B) Nonhuman primate neural progenitor cells (NPCs) and (C) non-human primate primary neurons were treated with DMSO (vehicle) or CLM at indicated CLM concentrations (nM) for 2 h. (D) Wild-type iPSC-derived motor neuron and (E) primary human neurons were treated with DMSO or CLM at indicated concentrations (nM) for 2 h. Wild-type iPSC-derived motor neurons show clear p-H2AX activation following CLM treatment. RIPA

extracted whole cell lysates (B-E) were analyzed by immunoblotting using indicated antibodies: FUS, p-H2AX, GAPDH, tubulin. Refer to methods section for catalog numbers of the specific antibodies used. GAPDH and Tubulin are used as loading controls to verify equal protein loading. Position of molecular weight markers (kDa) labeled on left side of each immunoblot.

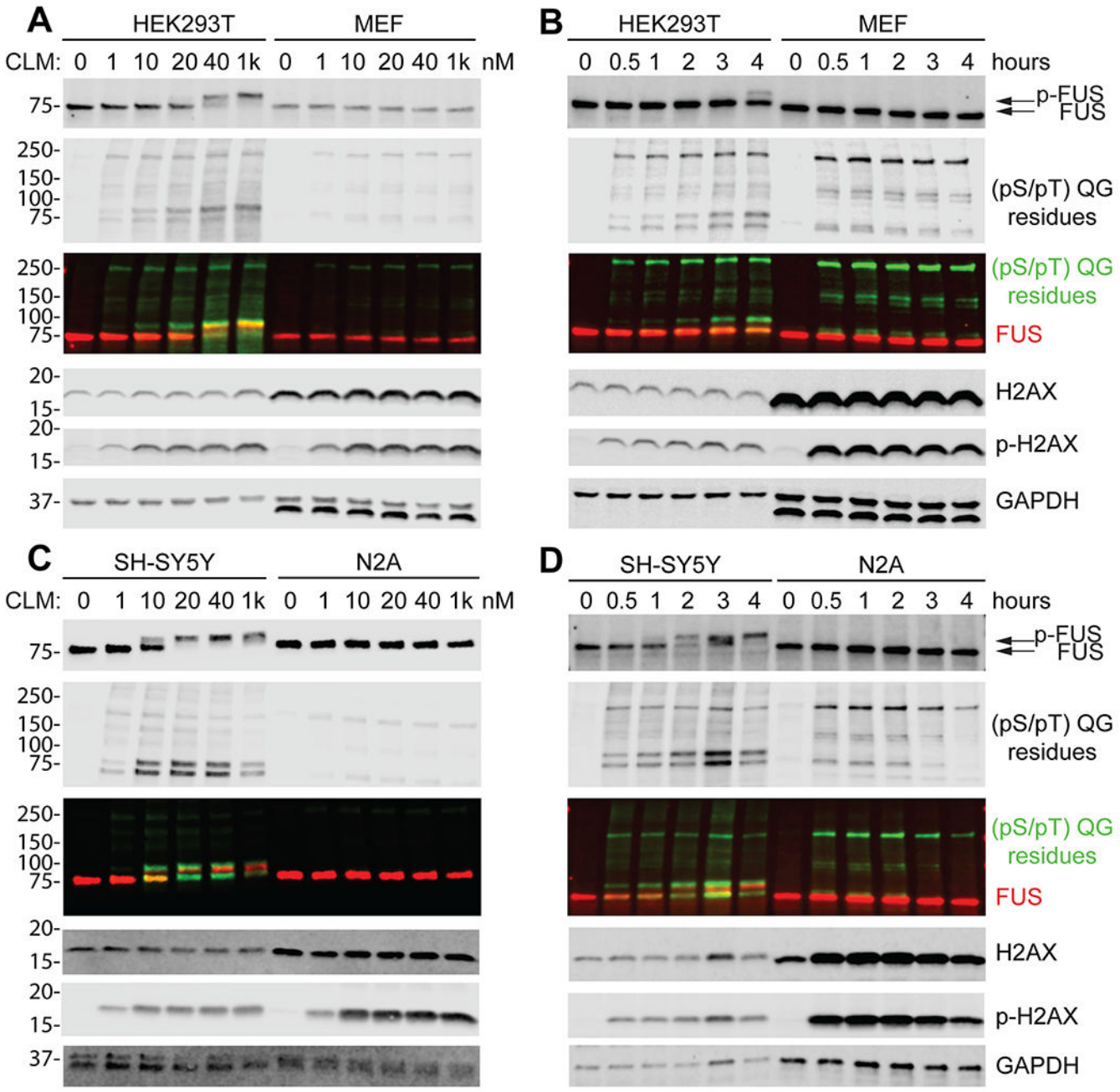

Fig. 2.

FUS is phosphorylated following CLM treatment in immortalized cell lines of human origin but not mouse. In human embryonic kidney (HEK293T) cells there is a (A) dose and (B) time dependent increase in phosphorylated FUS in response to CLM treatment. In contrast, phosphorylated FUS is undetectable in MEF cells at all tested doses and times. HEK293T and mouse embryonic fibroblasts (MEF) were treated with increasing concentrations (nM) of CLM for 2 h (A) or 10 nM CLM for 0 to 4 h (B). Similar to HEK293T cells, SH-SY5Y, a human neuroblastoma cell lines, displays a (C) dose and (D) time dependent increase in phosphorylated FUS following CLM treatment. In contrast, the appearance of

phosphorylated FUS after CLM treatment is undetectable in Neuro2A (N2A) cells, a mouse neuroblastoma cell lines. SH-SY5Y and N2A cells were treated with increasing concentrations of CLM for 2 h (C) or 20 nM CLM for 0–4 h (D). All control cells (0) were treated with the vehicle, DMSO, for either 2 (A, C) or 4 (B, D) hours. RIPA extracted whole cell lysates were analyzed with indicated antibodies: FUS, (pS/pT) QG residues, H2AX, p-H2AX, and GAPDH. p-H2AX activation, a marker of double strand DNA damage, occurs in all cells treated with CLM regardless of species. GAPDH is used as a loading control.

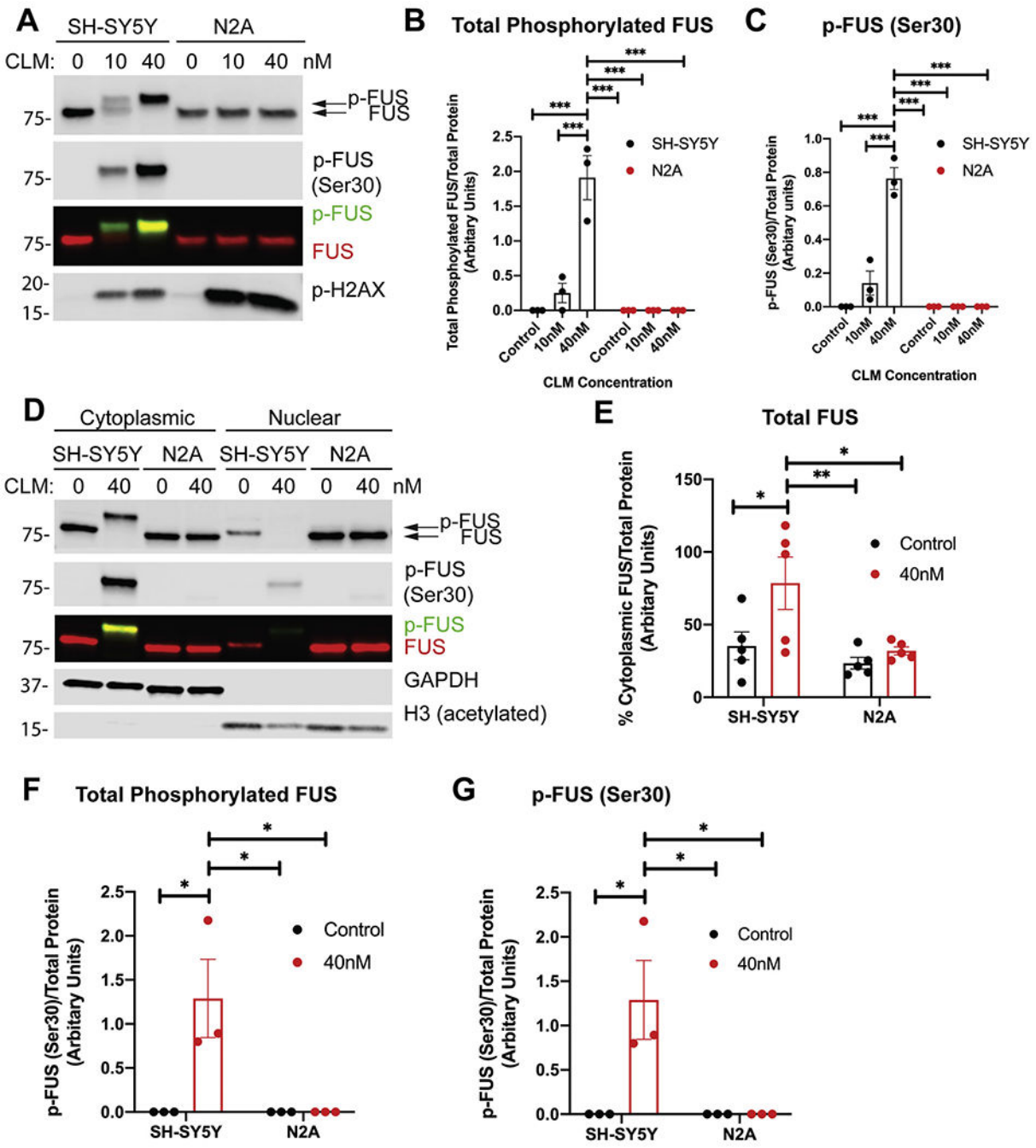

Fig. 3.

FUS is not phosphorylated or re-localized to the cytoplasm in mouse cells following CLM treatment. Human derived SH-SY5Y cells and mouse derived N2A cells were directly compared by western blot. (A) SH-SY5Y and N2A cells were treated with increasing doses of CLM for 2 h. Following treatment, RIPA extracted whole cell lysate was analyzed using the following antibodies: FUS, p-FUS (Ser30), and p-H2AX. (B) Quantification of (A) for phosphorylation of FUS (top band) at different concentrations of CLM were normalized to total protein. (C) Quantification of (A) for phosphorylation of FUS at residue Ser30 at

different concentrations of CLM were normalized to total protein. Error bars indicate mean ± SEM (n = 3). (D) SH-SY5Y and N2A cells were treated with increasing doses of CLM for 2 h. Cytoplasmic and nuclear fractions were collected and analyzed by western blot using the following antibodies: FUS, p-FUS (Ser30), GAPDH and H3. GAPDH and H3 were used as markers for cytoplasmic and nuclear fractions, respectively. (E) Quantification of (D) for the percentage of FUS found within the cytoplasmic fraction was normalized to total protein. (F) Quantification of (D) showing phosphorylation of FUS (top band) at different concentrations of CLM was normalized to total protein. (G) Quantification of (D) for phosphorylation of FUS at residue Ser30 at different concentrations of CLM was normalized to total protein. Error bars indicate mean ± SEM (n = 5). All control cells (0) received DMSO for 2 h.

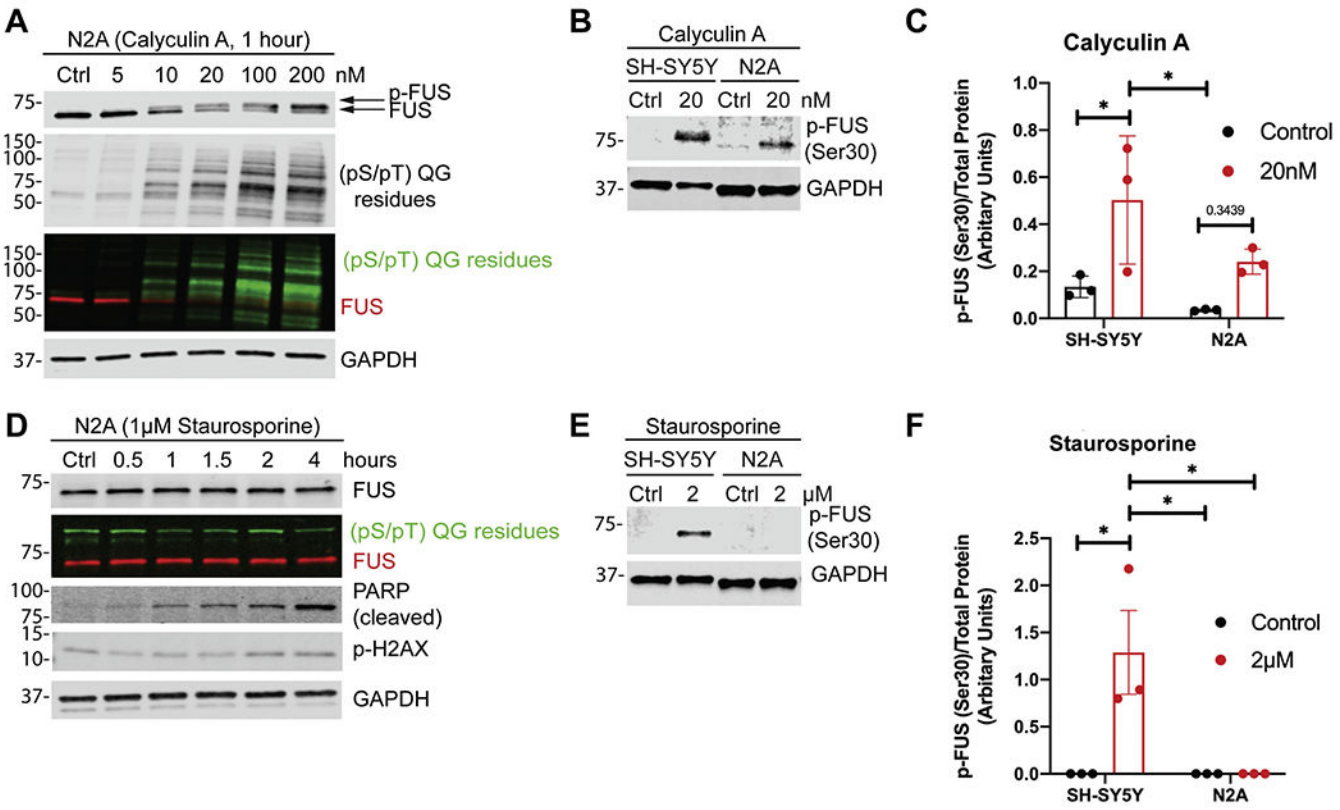

Fig. 4.

Neither calyculin A or staurosporine induces robust phosphorylation of mouse FUS. Calyculin A, an inhibitor of protein phosphatases PP1 and PP2A, causes a minor dose dependent increase in phosphorylated FUS (p-FUS) in mouse-derived cells. (A) Neuro2A (N2A) cells were treated with either the vehicle, DMSO (0), or increasing doses of Calyculin A for 1 h. RIPA extracted whole cells lysates were analyzed with indicated antibodies: FUS, p-Ser/Thr, and GAPDH. (A) N2A and SH-SY5Y cells were treated with 20 nM Cal A for 15 min. (C) Samples shown in (B) were quantified and normalized to total protein. Error bars indicate mean ± SEM (n = 3). All control cells (0) received DMSO for 15 min. (D) N2A cells were treated with staurosporine, a nonselective inhibitor of protein kinases that causes double strand DNA damage and cell apoptosis, showed no indication of FUS phosphorylation response. PARP-1 cleavage is an indicator apoptosis and a known consequence of staurosporine treatment acts as a positive control for staurosporine treatment. RIPA extracted whole cell lysates were analyzed with indicated antibodies: FUS, p-Ser/Thr, mouse specific-PARP (cleaved) p-H2AX, and GAPDH. (E) N2A and SH-SY5Y cells were treated with 1 μM Staurosporine for 1.5 h. Cellular fractionation was performed to extract cytoplasmic proteins and detect p-FUS by western blotting. (F) Samples shown in (D) were quantified. Error bars indicate mean ± SEM (n = 3). All control cells (0) received DMSO for 1.5 h.

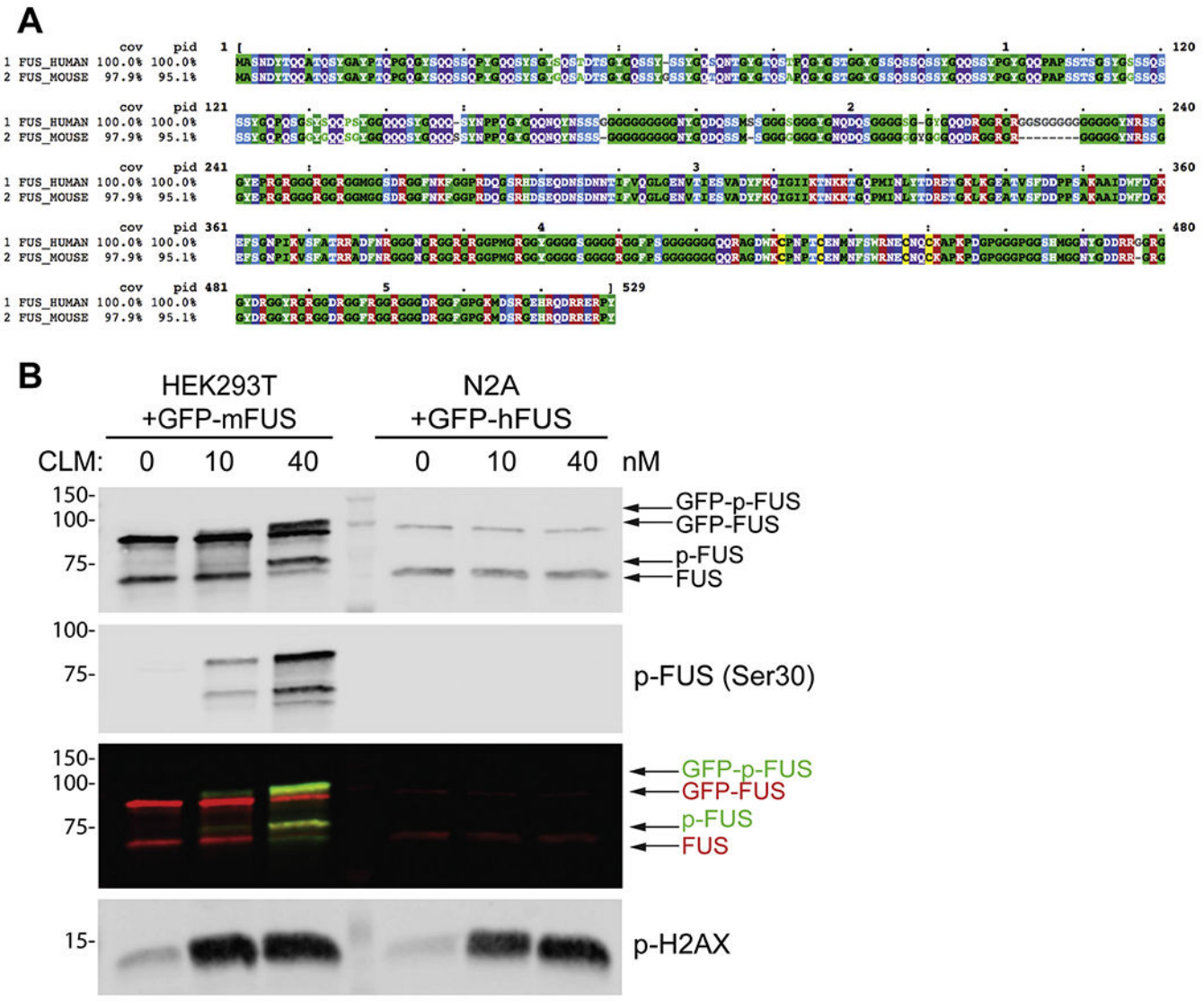

Fig. 5.

Mouse FUS can be phosphorylated in human cells following CLM treatment. We tested if mouse FUS can be phosphorylated in human cells following CLM treatment. Human and mouse FUS share ~95% sequence identity. (A) Graphical representation of amino acid sequence alignment for human (FUS_H) and mouse (FUS_M) FUS. Different colors indicate amino acid physical properties. Graphical representation was generated using Cluster Omega (Sievers et al., 2011). (B) GFP-tagged mouse FUS was transfected into HEK293T cells while GFP-tagged human FUS was transfected into N2A cells. GFP-tagged mouse FUS is phosphorylated when expressed in human cells treated with calicheamicin γ-1 (CLM). 24 h post transfection cells were treated with varying concentrations of CLM for 2 h and the whole cell lysate was harvested and analyzed with indicated antibodies: FUS, p-FUS (Ser 30), and p-H2AX. All control (0) cells received DMSO for 2 h.

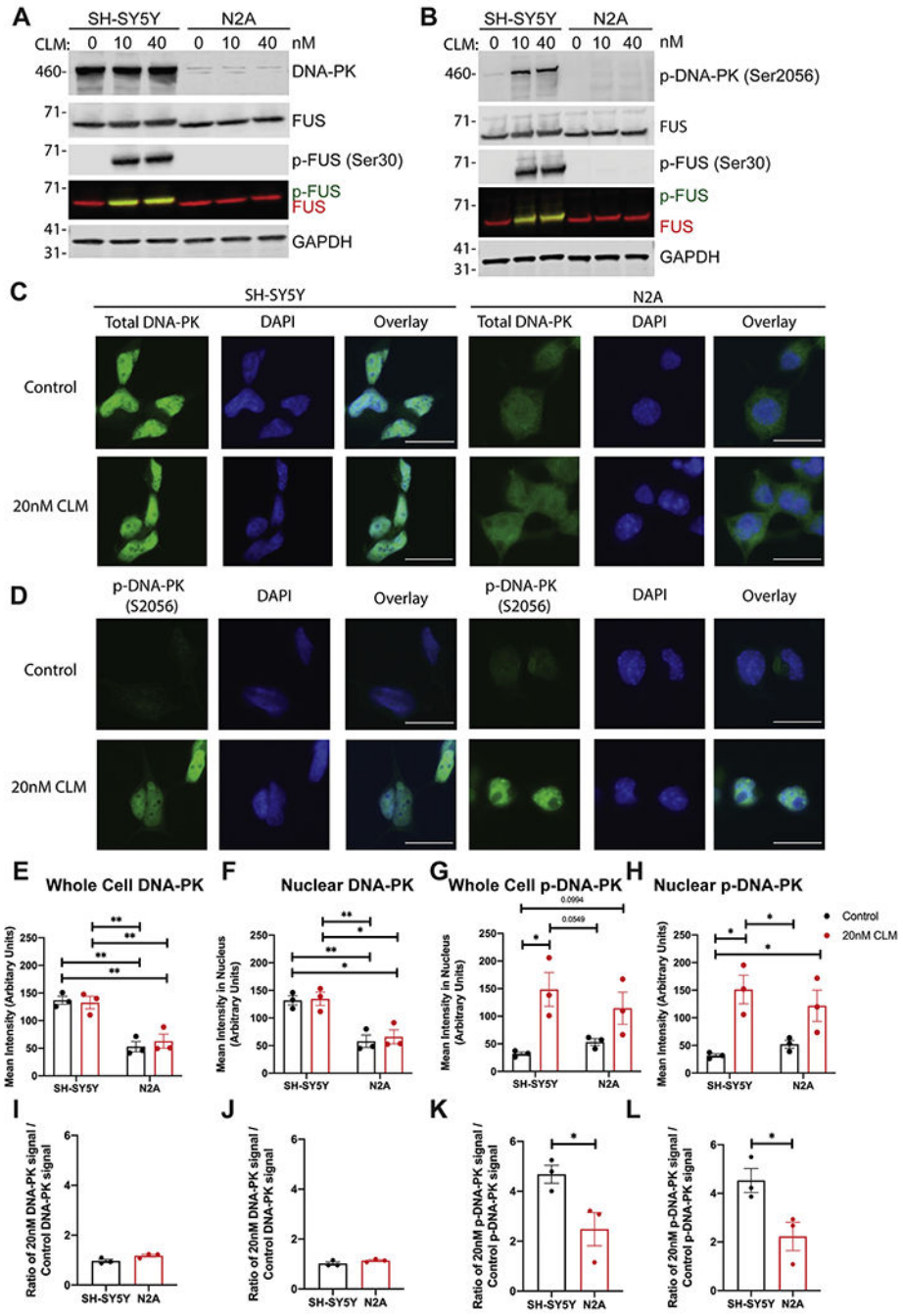

Fig. 6.

Compared to human cells, mouse cells have decreased levels of DNA-PK and activation following double strand DNA breaks induced by CLM treatment. SH-SY5Y cells show a distinct increase in activated DNA-PK whereas N2A cells lack a significant DNA-PK response following CLM treatment by western blot. SH-SY5Y and N2A cells were treated with increasing concentrations of CLM for 2 h. Following treatment, RIPA extracted whole cell lysates were analyzed for (A) total and (B) activated DNA-PK signal using the following antibodies: DNA-PK, p-DNA-PK, FUS, p-FUS (Ser30), and GAPDH. (C/D) N2A

cells have lower total and activated DNA-PK following CLM as compared to SH-SY5Y cells by immunofluorescence. SH-SY5Y and N2A cells were treated with DMSO (control) or CLM (20 nM CLM) for 2 h and stained for (C) total and (D) activated DNA-PK. Nuclei were counter-stained with DAPI. Four images with an average of 527 cells each were used for quantification per replicate (n = 3). Total and activated DNA-PK signal was quantified for both the (E/G) whole cell and (F/H) nucleus. SH-SY5Y cells show robust (E/F) total and (G/H) activated DNA-PK (p-DNA-PK, S2056) signal following CLM while N2A cell signal remains modest in presence of CLM. (I/J/K/L)The ratio of the signal from treated (20 nM CLM) to the signal from untreated (control) cells was calculated for each graph. Error bars on graphs indicate mean ± SEM.